

---

# Stabilizing Training of Generative Adversarial Networks through Regularization

---

**Kevin Roth**

Department of Computer Science  
ETH Zürich  
kevin.roth@inf.ethz.ch

**Aurelien Lucchi**

Department of Computer Science  
ETH Zürich  
aurelien.lucchi@inf.ethz.ch

**Sebastian Nowozin**

Microsoft Research  
Cambridge, UK  
sebastian.nowozin@microsoft.com

**Thomas Hofmann**

Department of Computer Science  
ETH Zürich  
thomas.hofmann@inf.ethz.ch

## Abstract

Deep generative models based on Generative Adversarial Networks (GANs) have demonstrated impressive sample quality but in order to work they require a careful choice of architecture, parameter initialization, and selection of hyper-parameters. This fragility is in part due to a dimensional mismatch or non-overlapping support between the model distribution and the data distribution, causing their density ratio and the associated  $f$ -divergence to be undefined. We overcome this fundamental limitation and propose a new regularization approach with low computational cost that yields a stable GAN training procedure. We demonstrate the effectiveness of this regularizer across several architectures trained on common benchmark image generation tasks. Our regularization turns GAN models into reliable building blocks for deep learning.<sup>1</sup>

## 1 Introduction

A recent trend in the world of generative models is the use of deep neural networks as data generating mechanisms. Two notable approaches in this area are variational auto-encoders (VAEs) [14, 28] as well as generative adversarial networks (GAN) [8]. GANs are especially appealing as they move away from the common likelihood maximization viewpoint and instead use an adversarial game approach for training generative models. Let us denote by  $\mathbb{P}(\mathbf{x})$  and  $\mathbb{Q}_\theta(\mathbf{x})$  the data and model distribution, respectively. The basic idea behind GANs is to pair up a  $\theta$ -parametrized generator network that produces  $\mathbb{Q}_\theta$  with a discriminator which aims to distinguish between  $\mathbb{P}$  and  $\mathbb{Q}_\theta$ , whereas the generator aims for making  $\mathbb{Q}_\theta$  indistinguishable from  $\mathbb{P}$ . Effectively the discriminator represents a class of objective functions  $\mathcal{F}$  that measures dissimilarity of pairs of probability distributions. The final objective is then formed via a supremum over  $\mathcal{F}$ , leading to the saddle point problem

$$\min_{\theta} \left[ \ell(\mathbb{Q}_\theta; \mathcal{F}) := \sup_{F \in \mathcal{F}} F(\mathbb{P}, \mathbb{Q}_\theta) \right]. \quad (1)$$

The standard way of representing a specific  $\mathcal{F}$  is through a family of statistics or discriminants  $\phi \in \Phi$ , typically realized by a neural network [8, 26]. In GANs, we use these discriminators in a logistic classification loss as follows

$$F(\mathbb{P}, \mathbb{Q}; \phi) = \mathbf{E}_{\mathbb{P}} [g(\phi(\mathbf{x}))] + \mathbf{E}_{\mathbb{Q}} [g(-\phi(\mathbf{x}))], \quad (2)$$

---

<sup>1</sup>Code available at [https://github.com/rothk/Stabilizing\\_GANs](https://github.com/rothk/Stabilizing_GANs)

where  $g(z) = \ln(\sigma(z))$  is the log-logistic function (for reference,  $\sigma(\phi(\mathbf{x})) = D(\mathbf{x})$  in [8]).

As shown in [8], for the Bayes-optimal discriminator  $\phi^* \in \Phi$ , the above generator objective reduces to the Jensen-Shannon (JS) divergence between  $\mathbb{P}$  and  $\mathbb{Q}$ . The work of [25] later generalized this to a more general class of  $f$ -divergences, which gives more flexibility in cases where the generative model may not be expressive enough or where data may be scarce.

We consider three different challenges for learning the model distribution:

(A) *empirical estimation*: the model family may contain the true distribution or a good approximation thereof, but one has to identify it based on a finite training sample drawn from  $\mathbb{P}$ . This is commonly addressed by the use of regularization techniques to avoid overfitting, e.g. in the context of estimating  $f$ -divergences with  $M$ -estimators [24]. In our work, we suggest a novel (Tikhonov) regularizer, derived and motivated from a training-with-noise scenario, where  $\mathbb{P}$  and  $\mathbb{Q}$  are convolved with white Gaussian noise [30, 3], namely

$$F_\gamma(\mathbb{P}, \mathbb{Q}; \phi) := F(\mathbb{P} * \Lambda, \mathbb{Q} * \Lambda; \phi), \quad \Lambda = \mathcal{N}(\mathbf{0}, \gamma \mathbf{I}). \quad (3)$$

(B) *density misspecification*: the model distribution and true distribution both have a density function with respect to the same base measure but there exists no parameter for which these densities are sufficiently similar. Here, the principle of parameter estimation via divergence minimization is provably sound in that it achieves a well-defined limit [1, 21]. It therefore provides a solid foundation for statistical inference that is robust with regard to model misspecifications.

(C) *dimensional misspecification*: the model distribution and the true distribution do not have a density function with respect to the same base measure or – even worse –  $\text{supp}(\mathbb{P}) \cap \text{supp}(\mathbb{Q})$  may be negligible. This may occur, whenever the model and/or data are confined to low-dimensional manifolds [3, 23]. As pointed out in [3], a geometric mismatch can be detrimental for  $f$ -GAN models as the resulting  $f$ -divergence is not finite (the sup in Eq. (1) is  $+\infty$ ). As a remedy, it has been suggested to use an alternative family of distance functions known as *integral probability metrics* [22, 31]. These include the Wasserstein distance used in Wasserstein GANs (WGAN) [3] as well as RKHS-induced maximum mean discrepancies [9, 16, 6], which all remain well-defined. We will provide evidence (analytically and experimentally) that the noise-induced regularization method proposed in this paper effectively makes  $f$ -GAN models robust against dimensional misspecifications. While this introduces some dependency on the (Euclidean) metric of the ambient data space, it does so on a well-controlled length scale (the amplitude of noise or strength of the regularization  $\gamma$ ) and by retaining the benefits of  $f$ -divergences. This is a rather gentle modification compared to the more radical departure taken in Wasserstein GANs, which rely solely on the ambient space metric (through the notion of optimal mass transport).

In what follows, we will take Eq. (3) as the starting point and derive an approximation via a regularizer that is simple to implement as an integral operator penalizing the squared gradient norm. As opposed to a naïve norm penalization, each  $f$ -divergence has its own characteristic weighting function over the input space, which depends on the discriminator output. We demonstrate the effectiveness of our approach on a simple Gaussian mixture as well as on several benchmark image datasets commonly used for generative models. In both cases, our proposed regularization yields stable GAN training and produces samples of higher visual quality. We also perform pairwise tests of regularized vs. unregularized GANs using a novel *cross-testing protocol*.

In summary, we make the following contributions:

- We systematically derive a novel, efficiently computable regularization method for  $f$ -GAN.
- We show how this addresses the dimensional misspecification challenge.
- We empirically demonstrate stable GAN training across a broad set of models.

## 2 Background

The fundamental way to learn a generative model in machine learning is to (i) define a parametric family of probability densities  $\{\mathbb{Q}_\theta\}$ ,  $\theta \in \Theta \subseteq \mathbb{R}^d$ , and (ii) find parameters  $\theta^* \in \Theta$  such that  $\mathbb{Q}_{\theta^*}$  is closest (in some sense) to the true distribution  $\mathbb{P}$ . There are various ways to measure how close model and real distribution are, or equivalently, various ways to define a distance or divergence function between  $\mathbb{P}$  and  $\mathbb{Q}$ . In the following we review different notions of divergences used in the literature.

**$f$ -divergence.** GANs [8] are known to minimize the Jensen-Shannon divergence between  $\mathbb{P}$  and  $\mathbb{Q}$ . This was generalized in [25] to  $f$ -divergences induced by a convex functions  $f$ . An interesting property of  $f$ -divergences is that they permit a variational characterization [24, 27] via

$$D_f(\mathbb{P}||\mathbb{Q}) := \mathbf{E}_{\mathbb{Q}} \left[ f \circ \frac{d\mathbb{P}}{d\mathbb{Q}} \right] = \int_{\mathcal{X}} \sup_u \left( u \cdot \frac{d\mathbb{P}}{d\mathbb{Q}} - f^c(u) \right) d\mathbb{Q}, \quad (4)$$

where  $d\mathbb{P}/d\mathbb{Q}$  is the Radon-Nikodym derivative and  $f^c(t) \equiv \sup_{u \in \text{dom}_f} \{ut - f(u)\}$  is the *Fenchel dual* of  $f$ . By defining an arbitrary class of statistics  $\Psi \ni \psi : \mathcal{X} \rightarrow \mathbb{R}$  we arrive at the bound

$$D_f(\mathbb{P}||\mathbb{Q}) \geq \sup_{\psi} \int \left( \psi \cdot \frac{d\mathbb{P}}{d\mathbb{Q}} - f^c \circ \psi \right) d\mathbb{Q} = \sup_{\psi} \{ \mathbf{E}_{\mathbb{P}}[\psi] - \mathbf{E}_{\mathbb{Q}}[f^c \circ \psi] \}. \quad (5)$$

Eq. (5) thus gives us a variational lower bound on the  $f$ -divergence as an expectation over  $\mathbb{P}$  and  $\mathbb{Q}$ , which is easier to evaluate (e.g. via sampling from  $\mathbb{P}$  and  $\mathbb{Q}$ , respectively) than the density based formulation. We can see that by identifying  $\psi = g \circ \phi$  and with the choice of  $f$  such that  $f^c = -\ln(1 - \exp)$ , we get  $f^c \circ \psi = -\ln(1 - \sigma(\phi)) = -g(-\phi)$  thus recovering Eq. (2).

**Integral Probability Metrics (IPM).** An alternative family of divergences are integral probability metrics [22, 31], which find a witness function to distinguish between  $\mathbb{P}$  and  $\mathbb{Q}$ . This class of methods yields an objective similar to Eq. (2) that requires optimizing a distance function between two distributions over a function class  $\mathcal{F}$ . Particular choices for  $\mathcal{F}$  yield the kernel maximum mean discrepancy approach of [9, 16] or Wasserstein GANs [3]. The latter distance is defined as

$$W(\mathbb{P}, \mathbb{Q}) = \sup_{\|f\|_L \leq 1} \{ \mathbf{E}_{\mathbb{P}}[f] - \mathbf{E}_{\mathbb{Q}}[f] \}, \quad (6)$$

where the supremum is taken over functions  $f$  which have a bounded Lipschitz constant.

As shown in [3], the Wasserstein metric implies a different notion of convergence compared to the JS divergence used in the original GAN. Essentially, the Wasserstein metric is said to be *weak* as it requires the use of a weaker topology, thus making it easier for a sequence of distribution to converge. The use of a weaker topology is achieved by restricting the function class to the set of bounded Lipschitz functions. This yields a hard constraint on the function class that is empirically hard to satisfy. In [3], this constraint is implemented via weight clipping, which is acknowledged to be a "terrible way" to enforce the Lipschitz constraint. As will be shown later, our regularization penalty can be seen as a soft constraint on the Lipschitz constant of the function class which is easy to implement in practice. Recently, [10] has also proposed a similar regularization; while their proposal was motivated for Wasserstein GANs and does not extend to  $f$ -divergences it is interesting to observe that both their and our regularization work on the gradient.

**Training with Noise.** As suggested in [3, 30], one can break the dimensional misspecification discussed in Section 1 by adding continuous noise to the inputs of the discriminator, therefore smoothing the probability distribution. However, this requires to add high-dimensional noise, which introduces significant variance in the parameter estimation process. Counteracting this requires a lot of samples and therefore ultimately leads to a costly or impractical solution. Instead we propose an approach that relies on analytic convolution of the densities  $\mathbb{P}$  and  $\mathbb{Q}$  with Gaussian noise. As we demonstrate below, this yields a simple weighted penalty function on the norm of the gradients. Conceptually we think of this noise not as being part of the generative process (as in [3]), but rather as a way to define a smoother family of discriminants for the variational bound of  $f$ -divergences.

**Regularization for Mode Dropping.** Other regularization techniques address the problem of mode dropping and are complementary to our approach. This includes the work of [7] which incorporates a supervised training signal as a regularizer on top of the discriminator target. To implement supervision the authors use an additional auto-encoder as well as a two-step training procedure which might be computationally expensive. A similar approach was proposed by [20] that stabilizes GANs by unrolling the optimization of the discriminator. The main drawback of this approach is that the computational cost scales with the number of unrolling steps. In general, it is not clear to what extent these methods not only stabilize GAN training, but also address the conceptual challenges listed in Section 1.

### 3 Noise-Induced Regularization

From now onwards, we consider the general  $f$ -GAN [25] objective defined as

$$F(\mathbb{P}, \mathbb{Q}; \psi) \equiv \mathbf{E}_{\mathbb{P}}[\psi] - \mathbf{E}_{\mathbb{Q}}[f^c \circ \psi]. \quad (7)$$

#### 3.1 Noise Convolution

From a practitioners point of view, training with noise can be realized by adding zero-mean random variables  $\xi$  to samples  $\mathbf{x} \sim \mathbb{P}, \mathbb{Q}$  during training. Here we focus on normal white noise  $\xi \sim \Lambda = \mathcal{N}(\mathbf{0}, \gamma \mathbf{I})$  (the same analysis goes through with a Laplacian noise distribution for instance). From a theoretical perspective, adding noise is tantamount to convolving the corresponding distribution as

$$\mathbf{E}_{\mathbb{P}} \mathbf{E}_{\Lambda}[\psi(\mathbf{x} + \xi)] = \int \psi(\mathbf{x}) \int p(\mathbf{x} - \xi) \lambda(\xi) d\xi d\mathbf{x} = \int \psi(\mathbf{x}) (p * \lambda)(\mathbf{x}) d\mathbf{x} = \mathbf{E}_{\mathbb{P} * \Lambda}[\psi]. \quad (8)$$

where  $p$  and  $\lambda$  are probability densities of  $\mathbb{P}$  and  $\Lambda$ , respectively, with regard to the Lebesgue measure. The noise distribution  $\Lambda$  as well as the resulting  $\mathbb{P} * \Lambda$  are guaranteed to have full support in the ambient space, i.e.  $\lambda(\mathbf{x}) > 0$  and  $(p * \lambda)(\mathbf{x}) > 0$  ( $\forall \mathbf{x}$ ). Technically, applying this to both  $\mathbb{P}$  and  $\mathbb{Q}$  makes the resulting generalized  $f$ -divergence well-defined, even when the generative model is dimensionally misspecified. Note that approximating  $\mathbf{E}_{\Lambda}$  through sampling was previously investigated in [30, 3].

#### 3.2 Convolved Discriminants

With symmetric noise,  $\lambda(\xi) = \lambda(-\xi)$ , we can write Eq. (8) equivalently as

$$\mathbf{E}_{\mathbb{P} * \Lambda}[\psi] = \mathbf{E}_{\mathbb{P}} \mathbf{E}_{\Lambda}[\psi(\mathbf{x} + \xi)] = \int p(\mathbf{x}) \int \psi(\mathbf{x} - \xi) \lambda(-\xi) d\xi d\mathbf{x} = \mathbf{E}_{\mathbb{P}}[\psi * \lambda]. \quad (9)$$

For the  $\mathbb{Q}$ -expectation in Eq. (7) one gets, by the same argument,  $\mathbf{E}_{\mathbb{Q} * \Lambda}[f^c \circ \psi] = \mathbf{E}_{\mathbb{Q}}[(f^c \circ \psi) * \lambda]$ . Formally, this generalizes the variational bound for  $f$ -divergences in the following manner:

$$F(\mathbb{P} * \Lambda, \mathbb{Q} * \Lambda; \psi) = F(\mathbb{P}, \mathbb{Q}; \psi * \lambda, (f^c \circ \psi) * \lambda), \quad F(\mathbb{P}, \mathbb{Q}; \rho, \tau) := \mathbf{E}_{\mathbb{P}}[\rho] - \mathbf{E}_{\mathbb{Q}}[\tau] \quad (10)$$

Assuming that  $\mathcal{F}$  is closed under  $\Lambda$  convolutions, the regularization will result in a relative weakening of the discriminator as we take the sup over a smaller, more regular family. Clearly, the low-pass effect of  $\Lambda$ -convolutions can be well understood in the Fourier domain. In this equivalent formulation, we leave  $\mathbb{P}$  and  $\mathbb{Q}$  unchanged, yet we change the view the discriminator can take on the ambient data space: metaphorically speaking, the generator is paired up with a short-sighted adversary.

#### 3.3 Analytic Approximations

In general, it may be difficult to analytically compute  $\psi * \lambda$  or – equivalently –  $\mathbf{E}_{\Lambda}[\psi(\mathbf{x} + \xi)]$ . However, for small  $\gamma$  we can use a Taylor approximation of  $\psi$  around  $\xi = 0$  (cf. [5]):

$$\psi(\mathbf{x} + \xi) = \psi(\mathbf{x}) + [\nabla \psi(\mathbf{x})]^T \xi + \frac{1}{2} \xi^T [\nabla^2 \psi(\mathbf{x})] \xi + \mathcal{O}(\xi^3) \quad (11)$$

where  $\nabla^2$  denotes the Hessian, whose trace  $\text{Tr}(\nabla^2) = \Delta$  is known as the Laplace operator. The properties of white noise result in the approximation

$$\mathbf{E}_{\Lambda}[\psi(\mathbf{x} + \xi)] = \psi(\mathbf{x}) + \frac{\gamma}{2} \Delta \psi(\mathbf{x}) + \mathcal{O}(\gamma^2) \quad (12)$$

and thereby lead directly to an approximation of  $F_{\gamma}$  (see Eq. (3)) via  $F = F_0$  plus a correction, i.e.

$$F_{\gamma}(\mathbb{P}, \mathbb{Q}; \psi) = F(\mathbb{P}, \mathbb{Q}; \psi) + \frac{\gamma}{2} \{ \mathbf{E}_{\mathbb{P}}[\Delta \psi] - \mathbf{E}_{\mathbb{Q}}[\Delta(f^c \circ \psi)] \} + \mathcal{O}(\gamma^2). \quad (13)$$

We can interpret Eq. (13) as follows: the Laplacian measures how much the scalar fields  $\psi$  and  $f^c \circ \psi$  differ at each point from their local average. It is thereby an infinitesimal proxy for the (exact) convolution.

The Laplace operator is a sum of  $d$  terms, where  $d$  is the dimensionality of the ambient data space. As such it does not suffer from the quadratic blow-up involved in computing the Hessian. If we realize the discriminator  $\psi$  via a deep network, however, then we need to be able to compute the Laplacian of composed functions. For concreteness, let us assume that  $\psi = h \circ G$ ,  $G = (g_1, \dots, g_k)$  and look



at a single input  $x$ , i.e.  $g_i : \mathbb{R} \rightarrow \mathbb{R}$ , then

$$(h \circ G)' = \sum_i g'_i \cdot (\partial_i h \circ G), \quad (h \circ G)'' = \sum_i g''_i \cdot (\partial_i h \circ G) + \sum_{i,j} g'_i \cdot g'_j \cdot (\partial_i \partial_j h \circ G) \quad (14)$$

So at the intermediate layer, we would need to effectively operate with a full Hessian, which is computationally demanding, as has already been observed in [5].

### 3.4 Efficient Gradient-Based Regularization

We would like to derive a (more) tractable strategy for regularizing  $\psi$ , which (i) avoids the detrimental variance that comes from sampling  $\xi$ , (ii) does not rely on explicitly convolving the distributions  $\mathbb{P}$  and  $\mathbb{Q}$ , and (iii) avoids the computation of Laplacians as in Eq. (13). Clearly, this requires to make further simplifications. We suggest to exploit properties of the maximizer  $\psi^*$  of  $F$  that can be characterized by [24]

$$(f^{c'} \circ \psi^*) d\mathbb{Q} = d\mathbb{P} \implies \mathbf{E}_{\mathbb{P}}[h] = \mathbf{E}_{\mathbb{Q}}[(f^{c'} \circ \psi^*) \cdot h] \quad (\forall h, \text{ integrable}). \quad (15)$$

The relevance of this becomes clear, if we apply the chain rule to  $\Delta(f^c \circ \psi)$ , assuming that  $f^c$  is twice differentiable

$$\Delta(f^c \circ \psi) = (f^{c''} \circ \psi) \cdot \|\nabla \psi\|^2 + (f^{c'} \circ \psi) \Delta \psi, \quad (16)$$

as now we get a convenient cancellation of the Laplacians at  $\psi = \psi^* + \mathcal{O}(\gamma)$

$$F_\gamma(\mathbb{P}, \mathbb{Q}; \psi^*) = F(\mathbb{P}, \mathbb{Q}; \psi^*) - \frac{\gamma}{2} \mathbf{E}_{\mathbb{Q}} \left[ (f^{c''} \circ \psi^*) \cdot \|\nabla \psi^*\|^2 \right] + \mathcal{O}(\gamma^2). \quad (17)$$

We can (heuristically) turn this into a regularizer by taking the leading terms,

$$F_\gamma(\mathbb{P}, \mathbb{Q}; \psi) \approx F(\mathbb{P}, \mathbb{Q}; \psi) - \frac{\gamma}{2} \Omega_f(\mathbb{Q}; \psi), \quad \Omega_f(\mathbb{Q}; \psi) := \mathbf{E}_{\mathbb{Q}} \left[ (f^{c''} \circ \psi) \cdot \|\nabla \psi\|^2 \right]. \quad (18)$$

Note that we do not assume that the Laplacian terms cancel far away from the optimum, i.e. we do not assume Eq. (15) to hold for  $\psi$  far away from  $\psi^*$ . Instead, the underlying assumption we make is that optimizing the gradient-norm regularized objective  $F_\gamma(\mathbb{P}, \mathbb{Q}; \psi)$  makes  $\psi$  converge to  $\psi^* + \mathcal{O}(\gamma)$ , for which we know that the Laplacian terms cancel [5, 2].

The convexity of  $f^c$  implies that the weighting function of the squared gradient norm is non-negative, i.e.  $f^{c''} \geq 0$ , which in turn implies that the regularizer  $-\frac{\gamma}{2} \Omega_f(\mathbb{Q}; \psi)$  is upper bounded (by zero). Maximization of  $F_\gamma(\mathbb{P}, \mathbb{Q}; \psi)$  with respect to  $\psi$  is therefore well-defined. Further considerations regarding the well-definedness of the regularizer can be found in sec. 7.2 in the Appendix.

## 4 Regularizing GANs

We have shown that training with noise is equivalent to regularizing the discriminator. Inspired by the above analysis, we propose the following class of  $f$ -GAN regularizers:

### Regularized $f$ -GAN

$$\begin{aligned} F_\gamma(\mathbb{P}, \mathbb{Q}; \psi) &= \mathbf{E}_{\mathbb{P}}[\psi] - \mathbf{E}_{\mathbb{Q}}[f^c \circ \psi] - \frac{\gamma}{2} \Omega_f(\mathbb{Q}; \psi) \\ \Omega_f(\mathbb{Q}; \psi) &:= \mathbf{E}_{\mathbb{Q}} \left[ (f^{c''} \circ \psi) \|\nabla \psi\|^2 \right] \end{aligned} \quad (19)$$

The regularizer corresponding to the commonly used parametrization of the Jensen-Shannon GAN can be derived analogously as shown in the Appendix. We obtain,

### Regularized Jensen-Shannon GAN

$$\begin{aligned} F_\gamma(\mathbb{P}, \mathbb{Q}; \varphi) &= \mathbf{E}_{\mathbb{P}}[\ln(\varphi)] + \mathbf{E}_{\mathbb{Q}}[\ln(1 - \varphi)] - \frac{\gamma}{2} \Omega_{JS}(\mathbb{P}, \mathbb{Q}; \varphi) \\ \Omega_{JS}(\mathbb{P}, \mathbb{Q}; \varphi) &:= \mathbf{E}_{\mathbb{P}} \left[ (1 - \varphi(\mathbf{x}))^2 \|\nabla \phi(\mathbf{x})\|^2 \right] + \mathbf{E}_{\mathbb{Q}} \left[ \varphi(\mathbf{x})^2 \|\nabla \phi(\mathbf{x})\|^2 \right] \end{aligned} \quad (20)$$

where  $\phi = \sigma^{-1}(\varphi)$  denotes the logit of the discriminator  $\varphi$ . We prefer to compute the gradient of  $\phi$  as it is easier to implement and more robust than computing gradients after applying the sigmoid.

---

**Algorithm 1 Regularized JS-GAN.** Default values:  $\gamma_0 = 2.0$ ,  $\alpha = 0.01$  (with annealing),  $\gamma = 0.1$  (without annealing),  $n_\varphi = 1$

---

**Require:** Initial noise variance  $\gamma_0$ , annealing decay rate  $\alpha$ , number of discriminator update steps  $n_\varphi$  per generator iteration, minibatch size  $m$ , number of training iterations  $T$

**Require:** Initial discriminator parameters  $\omega_0$ , initial generator parameters  $\theta_0$

**for**  $t = 1, \dots, T$  **do**

$\gamma \leftarrow \gamma_0 \cdot \alpha^{t/T}$  # annealing

**for**  $1, \dots, n_\varphi$  **do**

Sample minibatch of real data  $\{\mathbf{x}^{(1)}, \dots, \mathbf{x}^{(m)}\} \sim \mathbb{P}$ .

Sample minibatch of latent variables from prior  $\{\mathbf{z}^{(1)}, \dots, \mathbf{z}^{(m)}\} \sim p(\mathbf{z})$ .

$$F(\omega, \theta) = \frac{1}{m} \sum_{i=1}^m \left[ \ln \left( \varphi_\omega(\mathbf{x}^{(i)}) \right) + \ln \left( 1 - \varphi_\omega(G_\theta(\mathbf{z}^{(i)})) \right) \right]$$

$$\Omega(\omega, \theta) = \frac{1}{m} \sum_{i=1}^m \left[ \left( 1 - \varphi_\omega(\mathbf{x}^{(i)}) \right)^2 \|\nabla \phi_\omega(\mathbf{x}^{(i)})\|^2 + \varphi_\omega(G_\theta(\mathbf{z}^{(i)}))^2 \|\nabla_{\tilde{\mathbf{x}}} \phi_\omega(\tilde{\mathbf{x}})|_{\tilde{\mathbf{x}}=G_\theta(\mathbf{z}^{(i)})}\|^2 \right]$$

$$\omega \leftarrow \omega + \nabla_\omega \left( F(\omega, \theta) - \frac{\gamma}{2} \Omega(\omega, \theta) \right) \quad \# \text{gradient ascent}$$

**end for**

Sample minibatch of latent variables from prior  $\{\mathbf{z}^{(1)}, \dots, \mathbf{z}^{(m)}\} \sim p(\mathbf{z})$ .

$$F(\omega, \theta) = \frac{1}{m} \sum_{i=1}^m \ln \left( 1 - \varphi_\omega(G_\theta(\mathbf{z}^{(i)})) \right) \quad \text{or} \quad F_{\text{alt}}(\omega, \theta) = -\frac{1}{m} \sum_{i=1}^m \ln \left( \varphi_\omega(G_\theta(\mathbf{z}^{(i)})) \right)$$

$\theta \leftarrow \theta - \nabla_\theta F(\omega, \theta)$  # gradient descent

**end for**

The gradient-based updates can be performed with any gradient-based learning rule. We used Adam in our experiments.

---

## 4.1 Training Algorithm

Regularizing the discriminator provides an efficient way to convolve the distributions and is thereby sufficient to address the dimensional misspecification challenges outlined in the introduction. This leaves open the possibility to use the regularizer also in the objective of the generator. On the one hand, optimizing the generator through the regularized objective may provide useful gradient signal and therefore accelerate training. On the other hand, it destabilizes training close to convergence (if not dealt with properly), since the generator is incentivized to put probability mass where the discriminator has large gradients. In the case of JS-GANs, we recommend to pair up the regularized objective of the discriminator with the “alternative” or “non-saturating” objective for the generator, proposed in [8], which is known to provide strong gradients out of the box (see Algorithm 1).

## 4.2 Annealing

The regularizer variance  $\gamma$  lends itself nicely to annealing. Our experimental results indicate that a reasonable annealing scheme consists in regularizing with a large initial  $\gamma$  early in training and then (exponentially) decaying  $\gamma$  to a small non-zero value. We leave to future work the question of how to determine an optimal annealing schedule.

## 5 Experiments

### 5.1 2D submanifold mixture of Gaussians in 3D space

To demonstrate the stabilizing effect of the regularizer, we train a simple GAN architecture [20] on a 2D submanifold mixture of seven Gaussians arranged in a circle and embedded in 3D space (further details and an illustration of the mixture distribution are provided in the Appendix). We emphasize that this mixture is degenerate with respect to the base measure defined in ambient space as it does not have fully dimensional support, thus precisely representing one of the failure scenarios commonly

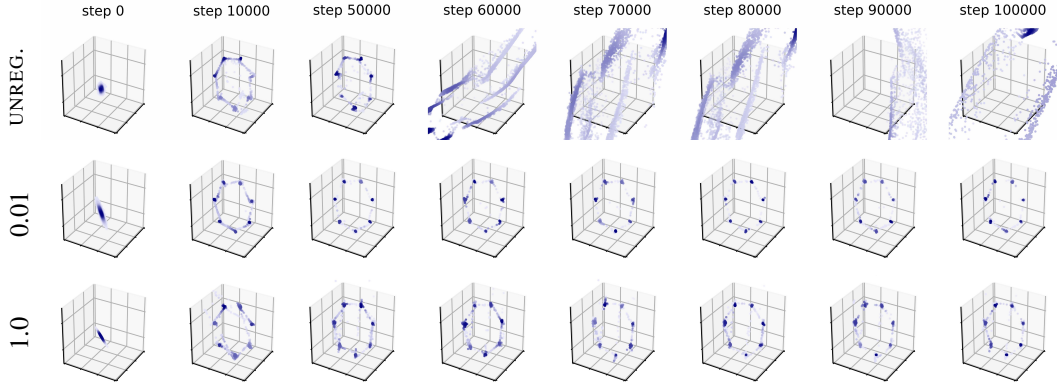


Figure 1: 2D submanifold mixture. The first row shows one of several unstable unregularized GANs trained to learn the dimensionally misspecified mixture distribution. The remaining rows show regularized GANs (with regularized objective for the discriminator and unregularized objective for the generator) for different levels of regularization  $\gamma$ . Even for small but non-zero noise variance, the regularized GAN can essentially be trained indefinitely without collapse. The color of the samples is proportional to the density estimated from a Gaussian KDE fit. The target distribution is shown in Fig. 5. GANs were trained with one discriminator update per generator update step (indicated).

described in the literature [3]. The results are shown in Fig. 1 for both standard unregularized GAN training as well as our regularized variant.

While the unregularized GAN collapses in literally every run after around 50k iterations, due to the fact that the discriminator concentrates on ever smaller differences between generated and true data (the stakes are getting higher as training progresses), the regularized variant can be trained essentially indefinitely (well beyond 200k iterations) without collapse for various degrees of noise variance, with and without annealing. The stabilizing effect of the regularizer is even more pronounced when the GANs are trained with five discriminator updates per generator update step, as shown in Fig. 6.

## 5.2 Stability across various architectures

To demonstrate the stability of the regularized training procedure and to showcase the excellent quality of the samples generated from it, we trained various network architectures on the CelebA [17], CIFAR-10 [15] and LSUN bedrooms [32] datasets. In addition to the deep convolutional GAN (DCGAN) of [26], we trained several common architectures that are known to be hard to train [4, 26, 19], therefore allowing us to establish a comparison to the concurrently proposed gradient-penalty regularizer for Wasserstein GANs [10]. Among these architectures are a DCGAN without any normalization in either the discriminator or the generator, a DCGAN with tanh activations and a deep residual network (ResNet) GAN [11]. We used the open-source implementation of [10] for our experiments on CelebA and LSUN, with one notable exception: we use batch normalization also for the discriminator (as our regularizer does not depend on the optimal transport plan or more precisely the gradient penalty being imposed along it).

All networks were trained using the Adam optimizer [13] with learning rate  $2 \times 10^{-4}$  and hyperparameters recommended by [26]. We trained all datasets using batches of size 64, for a total of 200K generator iterations in the case of LSUN and 100k iterations on CelebA. The results of these experiments are shown in Figs. 3 & 2. Further implementation details can be found in the Appendix.

## 5.3 Training time

We empirically found regularization to increase the overall training time by a marginal factor of roughly 1.4 (due to the additional backpropagation through the computational graph of the discriminator gradients). More importantly, however, (regularized)  $f$ -GANs are known to converge (or at least generate good looking samples) faster than their WGAN relatives [10].



Figure 2: *Stability across various architectures: ResNet, DCGAN, DCGAN without normalization and DCGAN with tanh activations (details in the Appendix). All samples were generated from regularized GANs with exponentially annealed  $\gamma_0 = 2.0$  (and alternative generator loss) as described in Algorithm 1. Samples were produced after 200k generator iterations on the LSUN dataset (see also Fig. 8 for a full-resolution image of the ResNet GAN). Samples for the unregularized architectures can be found in the Appendix.*



Figure 3: *Annealed Regularization. CelebA samples generated by (un)regularized ResNet GANs. The initial level of regularization  $\gamma_0$  is shown below each batch of images.  $\gamma_0$  was exponentially annealed as described in Algorithm 1. The regularized GANs can be trained essentially indefinitely without collapse, the superior quality is again evident. Samples were produced after 100k generator iterations.*

#### 5.4 Regularization vs. explicitly adding noise

We compare our regularizer against the common practitioner’s approach to explicitly adding noise to images during training. In order to compare both approaches (analytic regularizer vs. explicit noise), we fix a common batch size (64 in our case) and subsequently train with different noise-to-signal ratios (NSR): we take (batch-size/NSR) samples (both from the dataset and generated ones) to each of which a number of NSR noise vectors is added and feed them to the discriminator (so that overall both models are trained on the same batch size). We experimented with NSR 1, 2, 4, 8 and show the best performing ratio (further ratios in the Appendix). Explicitly adding noise in high-dimensional ambient spaces introduces additional sampling variance which is not present in the regularized variant. The results, shown in Fig. 4, confirm that the regularizer stabilizes across a broad range of noise levels and manages to produce images of considerably higher quality than the unregularized variants.

#### 5.5 Cross-testing protocol

We propose the following pairwise cross-testing protocol to assess the relative quality of two GAN models: unregularized GAN (*Model 1*) vs. regularized GAN (*Model 2*). We first report the confusion matrix (classification of 10k samples from the test set against 10k generated samples) for each model separately. We then classify 10k samples generated by *Model 1* with the discriminator of *Model 2* and vice versa. For both models, we report the fraction of false positives (FP) (Type I error) and false negatives (FN) (Type II error). The discriminator with the lower FP (and/or lower FN) rate defines the better model, in the sense that it is able to more accurately classify out-of-data samples, which indicates better generalization properties. We obtained the following results on CIFAR-10:





Figure 4: CIFAR-10 samples generated by (un)regularized DCGANs (with alternative generator loss), as well as by training a DCGAN with explicitly added noise (noise-to-signal ratio 4). The level of regularization or noise  $\gamma$  is shown above each batch of images. The regularizer stabilizes across a broad range of noise levels and manages to produce images of higher quality than the unregularized variants. Samples were produced after 50 training epochs.

#### Regularized GAN ( $\gamma = 0.1$ )

		True condition	
		Positive	Negative
Predicted	Positive	0.9688	0.0002
	Negative	0.0312	0.9998

Cross-testing: FP: 0.0

#### Unregularized GAN

		True condition	
		Positive	Negative
Predicted	Positive	1.0	0.0013
	Negative	0.0	0.9987

Cross-testing: FP: 1.0

For both models, the discriminator is able to recognize his own generator's samples (low FP in the confusion matrix). The regularized GAN also manages to perfectly classify the unregularized GAN's samples as fake (cross-testing FP 0.0) whereas the unregularized GAN classifies the samples of the regularized GAN as real (cross-testing FP 1.0). In other words, the regularized model is able to fool the unregularized one, whereas the regularized variant cannot be fooled.

## 6 Conclusion

We introduced a regularization scheme to train deep generative models based on generative adversarial networks (GANs). While dimensional misspecifications or non-overlapping support between the data and model distributions can cause severe failure modes for GANs, we showed that this can be addressed by adding a penalty on the weighted gradient-norm of the discriminator. Our main result is a simple yet effective modification of the standard training algorithm for GANs, turning them into reliable building blocks for deep learning that can essentially be trained indefinitely without collapse. Our experiments demonstrate that our regularizer improves stability, prevents GANs from overfitting and therefore leads to better generalization properties (cf cross-testing protocol). Further research on the optimization of GANs as well as their convergence and generalization can readily be built upon our theoretical results.

## Acknowledgements

We would like to thank Devon Hjelm for pointing out that the regularizer works well with ResNets. KR is thankful to Yannic Kilcher, Lars Mescheder, Paulina Grnarova and the dalab team for insightful discussions. Big thanks also to Ishaan Gulrajani and Taehoon Kim for their open-source GAN implementations. This work was supported by Microsoft Research through its PhD Scholarship Programme.

## References

- [1] Shun-ichi Amari and Hiroshi Nagaoka. *Methods of information geometry*. American Mathematical Soc., 2007.
- [2] Guozhong An. The effects of adding noise during backpropagation training on a generalization performance. *Neural Comput.*, pages 643–674, 1996.
- [3] Martin Arjovsky and Léon Bottou. Towards principled methods for training generative adversarial networks. In *ICLR*, 2017.
- [4] Martin Arjovsky, Soumith Chintala, and Léon Bottou. Wasserstein generative adversarial networks. In *PMLR*, Proceedings of Machine Learning Research, 2017.
- [5] Chris M Bishop. Training with noise is equivalent to tikhonov regularization. *Neural computation*, 7:108–116, 1995.
- [6] Diane Bouchacourt, Pawan K Mudigonda, and Sebastian Nowozin. Disco nets: Dissimilarity coefficients networks. In *Advances in Neural Information Processing Systems*, pages 352–360, 2016.
- [7] Tong Che, Yanran Li, Athul Paul Jacob, Yoshua Bengio, and Wenjie Li. Mode regularized generative adversarial networks. *arXiv preprint arXiv:1612.02136*, 2016.
- [8] Ian Goodfellow, Jean Pouget-Abadie, Mehdi Mirza, Bing Xu, David Warde-Farley, Sherjil Ozair, Aaron Courville, and Yoshua Bengio. Generative Adversarial Networks. In *Advances in Neural Information Processing Systems*, pages 2672–2680, 2014.
- [9] Arthur Gretton, Karsten M Borgwardt, Malte J Rasch, Bernhard Schölkopf, and Alexander Smola. A kernel two-sample test. *Journal of Machine Learning Research*, 13:723–773, 2012.
- [10] Ishaan Gulrajani, Faruk Ahmed, Martin Arjovsky, Vincent Dumoulin, and Aaron Courville. Improved training of wasserstein gans. In *Advances in Neural Information Processing Systems*, 2017.
- [11] Kaiming He, Xiangyu Zhang, Shaoqing Ren, and Jian Sun. Deep residual learning for image recognition. In *In IEEE Conference on Computer Vision and Pattern Recognition (CVPR)*, page 770–778, 2016.
- [12] Sergey Ioffe and Christian Szegedy. Batch normalization: Accelerating deep network training by reducing internal covariate shift. In *PMLR*, Proceedings of Machine Learning Research, pages 448–456, 2015.
- [13] Diederik P. Kingma and Jimmy Ba. Adam: A method for stochastic optimization. *The International Conference on Learning Representations (ICLR)*, 2014.
- [14] Diederik P Kingma and Max Welling. Auto-Encoding Variational Bayes. *The International Conference on Learning Representations (ICLR)*, 2013.
- [15] Alex Krizhevsky and Geoffrey Hinton. Learning multiple layers of features from tiny images. *CS UToronto*, 2009.
- [16] Yujia Li, Kevin Swersky, and Richard S Zemel. Generative moment matching networks. In *ICML*, pages 1718–1727, 2015.
- [17] Ziwei Liu, Ping Luo, Xiaogang Wang, and Xiaoou Tang. Deep learning face attributes in the wild. In *Proceedings of the IEEE International Conference on Computer Vision*, pages 3730–3738, 2015.
- [18] Ziwei Liu, Ping Luo, Xiaogang Wang, and Xiaoou Tang. Deep learning face attributes in the wild. In *Proceedings of International Conference on Computer Vision (ICCV)*, 2015.

- [19] Lars Mescheder, Sebastian Nowozin, and Andreas Geiger. The numerics of gans. In *Advances in Neural Information Processing Systems*, 2017.
- [20] Luke Metz, Ben Poole, David Pfau, and Jascha Sohl-Dickstein. Unrolled generative adversarial networks. In *International Conference on Learning Representations (ICLR)*, 2016.
- [21] Tom Minka. Divergence measures and message passing. Technical report, Microsoft Research, 2005.
- [22] Alfred Müller. Integral probability metrics and their generating classes of functions. *Advances in Applied Probability*, 29:429–443, 1997.
- [23] Hariharan Narayanan and Sanjoy Mitter. Sample complexity of testing the manifold hypothesis. In *Advances in Neural Information Processing Systems*, pages 1786–1794, 2010.
- [24] XuanLong Nguyen, Martin J Wainwright, and Michael I Jordan. Estimating divergence functionals and the likelihood ratio by convex risk minimization. *IEEE Transactions on Information Theory*, 56(11):5847–5861, 2010.
- [25] Sebastian Nowozin, Botond Cseke, and Ryota Tomioka. f-GAN: Training generative neural samplers using variational divergence minimization. In *Advances in Neural Information Processing Systems*, pages 271–279, 2016.
- [26] Alec Radford, Luke Metz, and Soumith Chintala. Unsupervised representation learning with deep convolutional generative adversarial networks. *arXiv preprint arXiv:1511.06434*, 2015.
- [27] Mark D Reid and Robert C Williamson. Information, divergence and risk for binary experiments. *Journal of Machine Learning Research*, 12:731–817, 2011.
- [28] Danilo J Rezende, Shakir Mohamed, and Daan Wierstra. Stochastic backpropagation and approximate inference in deep generative models. In *Proceedings of the 31st International Conference on Machine Learning*, 2014.
- [29] David W Scott. *Multivariate density estimation: theory, practice, and visualization*. John Wiley & Sons, 2015.
- [30] Casper Kaae Sønderby, Jose Caballero, Lucas Theis, Wenzhe Shi, and Ferenc Huszár. Amortised map inference for image super-resolution. *arXiv preprint arXiv:1610.04490*, 2016.
- [31] Bharath K Sriperumbudur, Kenji Fukumizu, Arthur Gretton, Bernhard Schölkopf, and Gert RG Lanckriet. On integral probability metrics, phi-divergences and binary classification. *arXiv preprint arXiv:0901.2698*, 2009.
- [32] Fisher Yu, Yinda Zhang, Shuran Song, Ari Seff, and Jianxiong Xiao. Lsun: Construction of a large-scale image dataset using deep learning with humans in the loop. *arXiv preprint arXiv:1506.03365*, 2015.

## 7 APPENDIX

### 7.1 Derivation of the Jensen-Shannon Regularizer.

The Jensen-Shannon GAN is typically encountered in one of two equivalent parametrizations: the commonly used “original” GAN parametrization [8],

$$\mathbf{E}_{\mathbb{P}} [\ln(\varphi)] + \mathbf{E}_{\mathbb{Q}} [\ln(1 - \varphi)] \quad (21)$$

and the Fenchel-dual  $f$ -GAN parametrization [25], where  $f^c = -\ln(1 - \exp)$ ,

$$\mathbf{E}_{\mathbb{P}} [\psi] - \mathbf{E}_{\mathbb{Q}} [f^c \circ \psi] = \mathbf{E}_{\mathbb{P}} [\psi] + \mathbf{E}_{\mathbb{Q}} [\ln(1 - \exp(\psi))] \quad (22)$$

Depending on whether we train the JS-GAN through its Fenchel-dual parametrization or with the original GAN objective we have to either use the regularizer in the general  $f$ -GAN form in Eq. (19), or in the specific Jensen-Shannon parametrization given in Eq. (20).

We now show how to derive the specific Jensen-Shannon regularizer, which is basically a repetition of the derivation of the general  $f$ -GAN regularizer presented in the main text. Using the same terminology and following the same line of thought as in section 3.3, i.e. assuming the noise variance is small, we can Taylor approximate the statistics  $\varphi$  around  $\boldsymbol{\xi} = 0$ ,

$$\varphi(\mathbf{x} + \boldsymbol{\xi}) = \varphi(\mathbf{x}) + [\nabla \varphi(\mathbf{x})] \boldsymbol{\xi} + \frac{1}{2} \boldsymbol{\xi}^T [\nabla^2 \varphi(\mathbf{x})] \boldsymbol{\xi} + \mathcal{O}(\boldsymbol{\xi}^3) \quad (23)$$

Expanding the noise convolved version of the objective in Eq. (21) and making use of the zero-mean and uncorrelatedness properties of the noise distribution, as well as applying the chain rule, we obtain

$$\begin{aligned} F_{\gamma}(\mathbb{P}, \mathbb{Q}; \varphi) &= \mathbf{E}_{\mathbb{P}} [\ln(\varphi)] + \mathbf{E}_{\mathbb{Q}} [\ln(1 - \varphi)] \\ &+ \frac{\gamma}{2} \left\{ \mathbf{E}_{\mathbb{P}} \left[ \frac{1}{\varphi} \Delta \varphi - \|\nabla \ln(\varphi)\|^2 \right] + \mathbf{E}_{\mathbb{Q}} \left[ -\frac{1}{1 - \varphi} \Delta \varphi - \|\nabla \ln(1 - \varphi)\|^2 \right] \right\} + \mathcal{O}(\gamma^2). \end{aligned} \quad (24)$$

Following the same arguments as in section 3.4, one can again show that the Laplacian terms cancel at  $\varphi = \varphi^* + \mathcal{O}(\gamma)$  and we arrive at

$$\begin{aligned} F_{\gamma}(\mathbb{P}, \mathbb{Q}; \varphi) &= \mathbf{E}_{\mathbb{P}} [\ln(\varphi)] + \mathbf{E}_{\mathbb{Q}} [\ln(1 - \varphi)] \\ &- \frac{\gamma}{2} \left\{ \mathbf{E}_{\mathbb{P}} [\|\nabla \ln(\varphi)\|^2] + \mathbf{E}_{\mathbb{Q}} [\|\nabla \ln(1 - \varphi)\|^2] \right\} + \mathcal{O}(\gamma^2), \end{aligned} \quad (25)$$

allowing us to read off the corresponding JS regularizer,

$$\begin{aligned} \Omega_{JS}(\mathbb{P}, \mathbb{Q}; \varphi) &= \mathbf{E}_{\mathbb{P}} [\|\nabla \ln \varphi(\mathbf{x})\|^2] + \mathbf{E}_{\mathbb{Q}} [\|\nabla \ln(1 - \varphi(\mathbf{x}))\|^2] \\ &= \mathbf{E}_{\mathbb{P}} \left[ \frac{1}{(\varphi(\mathbf{x}))^2} \|\nabla \varphi(\mathbf{x})\|^2 \right] + \mathbf{E}_{\mathbb{Q}} \left[ \frac{1}{(1 - \varphi(\mathbf{x}))^2} \|\nabla \varphi(\mathbf{x})\|^2 \right] \\ &= \mathbf{E}_{\mathbb{P}} \left[ \frac{1}{(\varphi(\mathbf{x}))^2} \|\sigma'(\phi(\mathbf{x})) \nabla \phi(\mathbf{x})\|^2 \right] + \mathbf{E}_{\mathbb{Q}} \left[ \frac{1}{(1 - \varphi(\mathbf{x}))^2} \|\sigma'(\phi(\mathbf{x})) \nabla \phi(\mathbf{x})\|^2 \right] \end{aligned} \quad (26)$$

In order to obtain the regularizer in the logit-parameterization, with  $\varphi(\mathbf{x}) = \sigma(\phi(\mathbf{x}))$ , we make use of the following property of the sigmoid

$$\sigma'(t) = \sigma(t)(1 - \sigma(t)) \quad (27)$$

which allows us to write

$$\Omega_{JS}(\mathbb{P}, \mathbb{Q}; \phi) = \mathbf{E}_{\mathbb{P}} [(1 - \varphi(\mathbf{x}))^2 \|\nabla \phi(\mathbf{x})\|^2] + \mathbf{E}_{\mathbb{Q}} [\varphi(\mathbf{x})^2 \|\nabla \phi(\mathbf{x})\|^2] \quad (28)$$

Let us finally also show that these two parametrizations are indeed equivalent at the optimum:

$$f^{c''}(t) = \frac{\exp(t)}{(1 - \exp(t))^2} \implies f^{c''}(\ln(\varphi^*)) = \frac{\varphi^*}{(1 - \varphi^*)^2} = \frac{\varphi^*}{1 - \varphi^*} + \frac{\varphi^{*2}}{(1 - \varphi^*)^2} \quad (29)$$

Thus,

$$\begin{aligned} f^{c''}(\ln(\varphi^*)) \|\nabla \ln(\varphi^*)\|^2 d\mathbb{Q} &= \left( \frac{\varphi^*}{1 - \varphi^*} + \frac{\varphi^{*2}}{(1 - \varphi^*)^2} \right) \|\nabla \ln(\varphi^*)\|^2 d\mathbb{Q} \\ &= \|\nabla \ln(\varphi^*)\|^2 d\mathbb{P} + \left\| \frac{\varphi^*}{1 - \varphi^*} \nabla \ln(\varphi^*) \right\|^2 d\mathbb{Q} \\ &= \|\nabla \ln(\varphi^*)\|^2 d\mathbb{P} + \|\nabla \ln(1 - \varphi^*)\|^2 d\mathbb{Q} \end{aligned} \quad (30)$$



## 7.2 Further Considerations Regarding the Regularizer

Following-up on our discussion of the regularizer in section 3.4: Due to a support or dimensionality mismatch we may have  $\sup F(\mathbb{P}, \mathbb{Q}; \psi) = +\infty$  and  $\psi^*$  may not exist. However, with  $\psi_\epsilon^*$  being the maximizer of  $F_\epsilon$  (which is guaranteed to exist for any  $\epsilon > 0$ ), we get

$$F_\gamma(\mathbb{P} * \mathcal{N}(\mathbf{0}, \epsilon \mathbf{I}), \mathbb{Q} * \mathcal{N}(\mathbf{0}, \epsilon \mathbf{I})) = F_\epsilon(\mathbb{P}, \mathbb{Q}; \psi_\epsilon^*) - \frac{\gamma}{2} \Omega_f(\mathbb{Q} * \mathcal{N}(\mathbf{0}, \epsilon \mathbf{I}); \psi_\epsilon^*) + \mathcal{O}(\gamma^2). \quad (31)$$

As  $\epsilon \rightarrow 0$ ,  $F_\epsilon$  may diverge and so may  $\|\nabla \psi_\epsilon^*\|$ . The sequence of regularizers  $\Omega_f(\mathbb{Q} * \mathcal{N}(\mathbf{0}, \epsilon \mathbf{I}); \cdot)$ , however, converges (at least pointwise) to a well defined limit, which is  $\Omega_f(\mathbb{Q}; \cdot)$ . This shows that the regularizer is well-defined even under dimensional misspecifications.

We can also justify the approximation in Eq. (18) more rigorously. Starting from the Taylor approximation of  $f^{c'}$  at  $\psi^*$ , we get pointwise

$$f^{c'} \circ \psi = f^{c'} \circ \psi^* + f^{c''} \circ (\psi - \psi^*) + \mathcal{O}(\|\psi - \psi^*\|^2) \quad (32)$$

So in first order of  $\|\psi - \psi^*\|_\infty$ , the approximation error is  $\Delta := \mathbf{E}_\mathbb{Q} [(f^{c''} \circ (\psi - \psi^*)) \cdot \Delta \psi]$ . Using Green’s identity, we can derive the following bound,  $\Delta \leq \mathcal{O}(L\delta)$ , where we assume  $|f^{c''}| \leq L$  and  $\|\nabla \psi - \nabla \psi^*\|_\infty < \delta$ . However, as this result only gives a formal guarantee for  $(\psi, \nabla \psi)$  sufficiently close to  $(\psi^*, \nabla \psi^*)$ , we refrain from presenting further technical details.

## 7.3 2D Submanifold Mixture of Gaussians in 3D Space

**Experimental Setup.** The experimental setup is inspired by the two-dimensional mixture of Gaussians in [20]. The dataset is constructed as follows. We sample from a mixture of seven Gaussians with standard deviation 0.01 and means equally spaced around the unit circle. This 2D mixture is then embedded in 3D space  $(x, y) \rightarrow (x, y, 0)$ , rotated by  $\pi/4$  around the axis  $(1, -1, 0)/\sqrt{2}$  and translated by  $(1, 1, 1)/\sqrt{3}$ . As illustrated in Fig. 5, this yields a mixture distribution that lives in a tilted 2D submanifold embedded in 3D space. It is important to emphasize that the mixture distribution is by design degenerate with respect to the base measure in 3D as it does not have full dimensional support. This precisely represents the dimensional misspecification scenario for GANs that we aim to address with our regularizer.

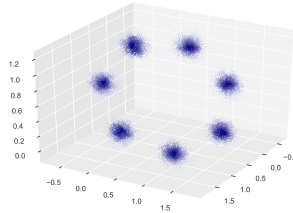


Figure 5: 2D submanifold mixture of Gaussians in 3D, obtained by embedding a two-dimensional mixture with means equally spaced around the unit circle in 3D ambient space. For visualization purposes, the standard deviation of the shown mixture components is 10x larger than the one used in the experiments. Samples are colored proportional to their density which we estimated from a Gaussian KDE with bandwidth selected using Scott’s rule [29].

**Architecture.** The architecture corresponds to the one used in [20] with one notable exception. We use 2 dimensional latent vectors  $z$ , sampled from a multivariate normal prior, (whereas [20] uses 256 dimensional  $z$ ), as we found lower dimensional latent variables greatly improve the performance of the unregularized GAN against which we compare. We did all experiments also for latent vectors of dimension 15: the obtained results are in accordance with those presented in the main text and below.

Both networks are optimized using Adam with a learning rate of  $1e-3$  and standard hyper-parameters. We trained on batches of size 512. Ten batches were generated to produce one image of the mixture at given time steps. The generator and discriminator network parameters were updated alternatively.

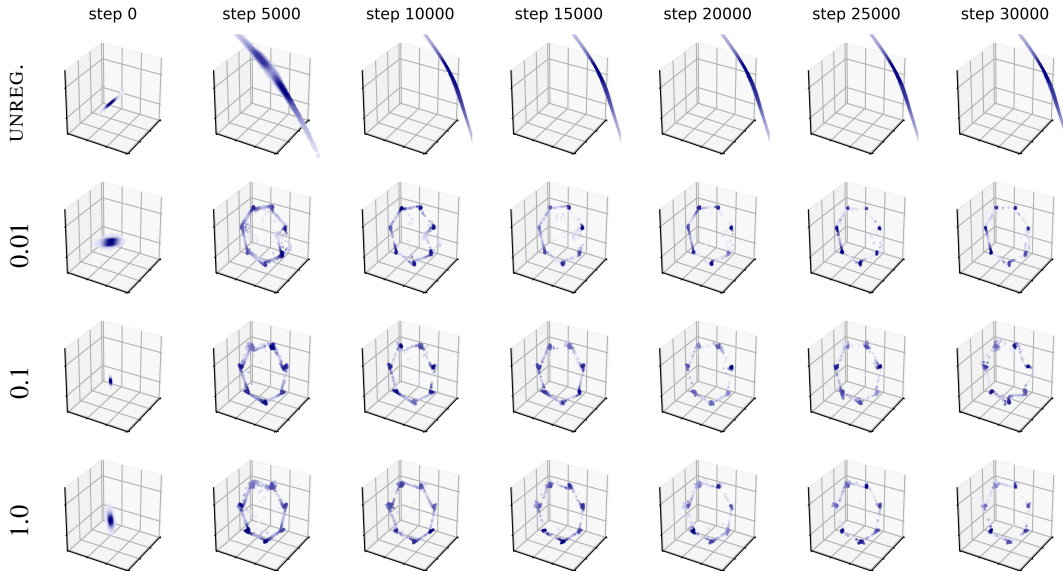


Figure 6: *2D submanifold mixture.* The first row shows one of several unstable unregularized GANs trying to learn the dimensionally misspecified mixture distribution. The remaining rows show regularized GANs (with regularized objective for the discriminator and unregularized objective for the generator) for different levels of regularization  $\gamma$ . Even for small but non-zero noise variance, the regularized GAN can essentially be trained indefinitely without collapse. The color of the samples is proportional to the density estimated from a Gaussian KDE fit. The target distribution is shown in Fig. 5. GANs were trained with five discriminator updates per generator update step (indicated).

#### 7.4 Image Datasets and Network Architectures

We trained on CelebA [18], CIFAR-10 [15] and LSUN [32]. All datasets were trained on minibatches of size 64. The respective GAN architectures are listed below.

**DCGAN.** For the CIFAR-10 experiments, we used the DCGAN (Deep Convolutional GAN) architecture of [26] implemented in Tensorflow by <https://github.com/carpedm20/DCGAN-tensorflow>.

For the LSUN experiments, we used the DCGAN architecture of [26] implemented in Tensorflow by [https://github.com/igul222/improved\\_wgan\\_training](https://github.com/igul222/improved_wgan_training).

In both cases, the discriminator uses batch normalization [12] in all but the first and last layer (except where explicitly stated otherwise). The generator uses batch normalization in all layers except the last one. The latent code is sampled from a 100-dimensional uniform distribution over  $[0, 1]$  (carpedm20) resp. 128-dimensional normal-(0,1) distribution (Gulrajani).

Both networks were trained using the Adam optimizer [13] (with hyper-parameters recommended by the DCGAN authors) for various different learning rates in the range  $[0.001, 0.0001]$ . The recommended learning rate  $2 \times 10^{-4}$  was found to perform best.

**ResNet GAN.** For the CelebA and LSUN experiments, we used a deep residual network ResNet [11] implemented in Tensorflow by [https://github.com/igul222/improved\\_wgan\\_training](https://github.com/igul222/improved_wgan_training) (implementation details can be found in [10]).

The ResNets use pre-activation residual blocks with two  $3 \times 3$  convolutional layers each and ReLU nonlinearities. The generator has one linear layer, followed by four residual blocks, one deconvolutional layer and tanh output activations. The discriminator has one convolutional layer, followed by four residual blocks and a linear output layer (the discriminator logits are then fed into the sigmoid GAN loss).

We use batch normalization [12] in the generator and discriminator (except explicitly stated otherwise). Both networks were optimized using Adam with learning rate  $2 \times 10^{-4}$  and standard hyperparameters. For further architectural details, please refer to [10] and the excellent open-source implementation referenced above.

### 7.5 Further Experimental Results.



Figure 7: Unregularized GANs (with alternative generator loss) across various architectures: ResNet, DCGAN, DCGAN without normalization and DCGAN with tanh activations. Samples were produced after 200k generator iterations on the LSUN dataset. Samples for the regularized architectures can be found in the main text. Some of these architectures are known to be hard to train.

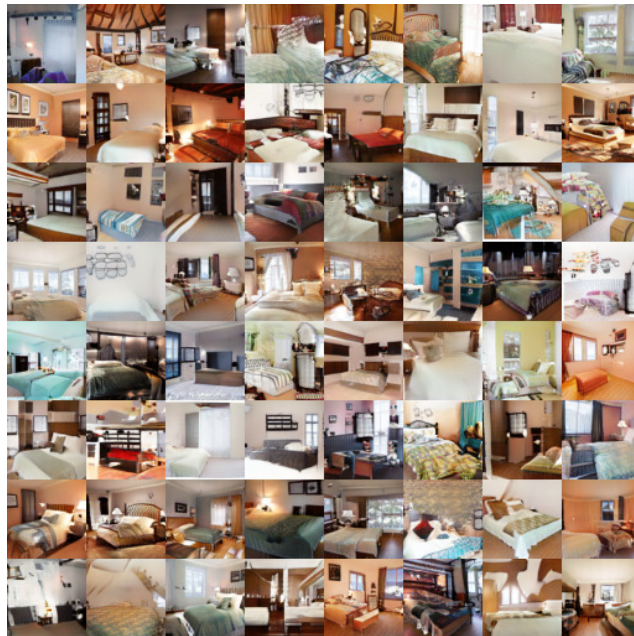


Figure 8: Regularized ResNet GAN. Full-resolution  $64 \times 64$  images generated by the regularized ResNet GAN after 200k generator iterations on the LSUN dataset. The initial level of regularization  $\gamma_0 = 2.0$  was exponentially annealed to  $\gamma_T = 0.01$ .



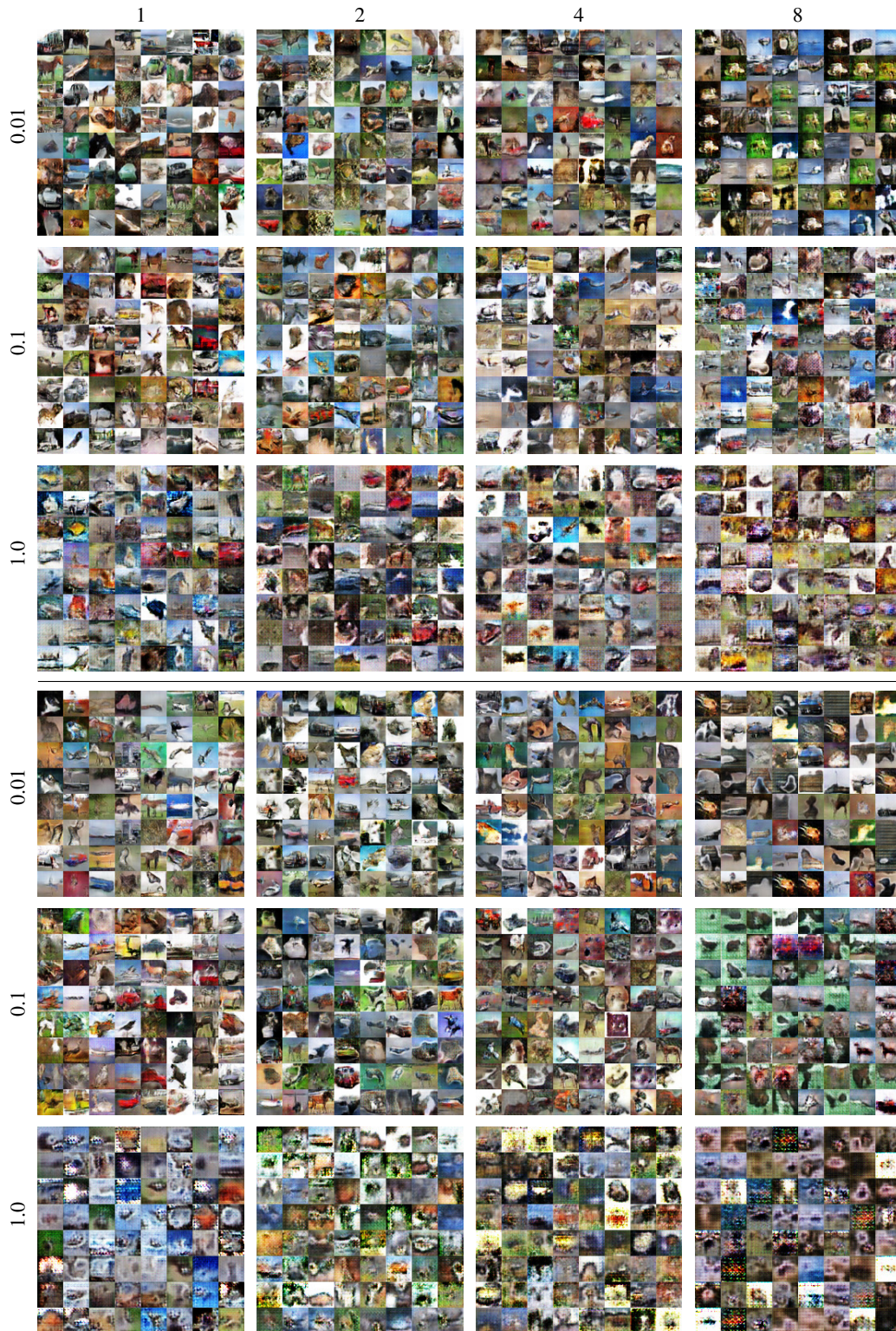


Figure 9: DCGAN trained with explicitly added noise. Top 3 rows: discriminator and generator trained with noise. Bottom 3 rows: discriminator is trained with noise while generator is trained without noise. White normal noise is added to images from the dataset as well as to samples from the generator during training. The generator was trained through the alternative loss. The level of noise  $\gamma$  is shown in the left most column, the different noise-to-signal ratios (NSR) above each column of images. Samples were produced after 50 training epochs.